HHS Public Access

Author manuscript

Curr Biol. Author manuscript; available in PMC 2021 July 29.

Published in final edited form as:

Curr Biol. 2021 July 26; 31(14): 2984–2994.e7. doi:10.1016/j.cub.2021.04.052.

RNA degradation is required for the germ-cell to maternal transition in *Drosophila*

Patrick Blatt[1], **Siu Wah Wong-Deyrup**[1], **Alicia McCarthy**[1,2], **Shane Breznak**[1], **Matthew D. Hurton**[3], **Maitreyi Upadhyay**[1,4], **Benjamin Bennink**[1], **Justin Camacho**[1], **Miler T. Lee**[*,3], **Prashanth Rangan**[*,#,1]

[1]University at Albany, Department of Biological Sciences, RNA Institute; 1400 Washington Avenue, LSRB 2033D, Albany, NY 12222

[2]10x Genomics, Inc., 6230 Stoneridge Mall Road, Pleasanton, CA, 94588

[3]University of Pittsburgh, Department of Biological Sciences; 4249 Fifth Avenue, Pittsburgh, PA 15260

[4]Department of Stem Cell and Regenerative Biology, Sherman Fairchild 100, Harvard University, 7 Divinity Avenue, Cambridge, MA 02138

Summary

In sexually reproducing animals, the oocyte contributes a large supply of RNAs that are essential to launch development upon fertilization. The mechanisms that regulate the composition of the maternal RNA contribution during oogenesis are unclear. Here, we show that a subset of RNAs expressed during the early stages of oogenesis is subjected to regulated degradation during oocyte specification. Failure to remove these RNAs results in oocyte dysfunction and death. We identify the RNA-degrading Super Killer complex and No-Go Decay factor Pelota as key regulators of oogenesis via targeted degradation of specific RNAs expressed in undifferentiated germ cells. These regulators target RNAs enriched for cytidine sequences that are bound by the polypyrimidine tract binding protein Half pint. Thus, RNA degradation helps orchestrate a germ cell-to-maternal transition that gives rise to the maternal contribution to the zygote.

Graphical Abstract

[*]Co-Corresponding authors: miler@pitt.edu & prangan@albany.edu, Twitter handle: @MTLeeLab and @RanganLab.
[#]Lead contact

Author contributions

Conceptualization, P.R., P.B., and M.T.L.; Methodology, P.R. and P.B.; Software, M.T.L. and M.D.H.; Formal Analysis, M.T.L., P.B. and M.D.H.; Investigation, P.B., S.W.-D., A.M., S.B., J.C., B.B., M.U.; Resources, P.B., S.W-D., and P.R.; Data Curation, P.B., and M.T.L.; Writing – Original Draft, P.R. and P.B.; Writing – Review & Editing, P.R., M.T.L. and P.B.; Visualization, P.B., and M.T.L.; Supervision, P.R.; Project Administration, P.R.; Funding Acquisition, P.R., P.B., and M.T.L.

Declaration of interests

The authors declare no competing interests.

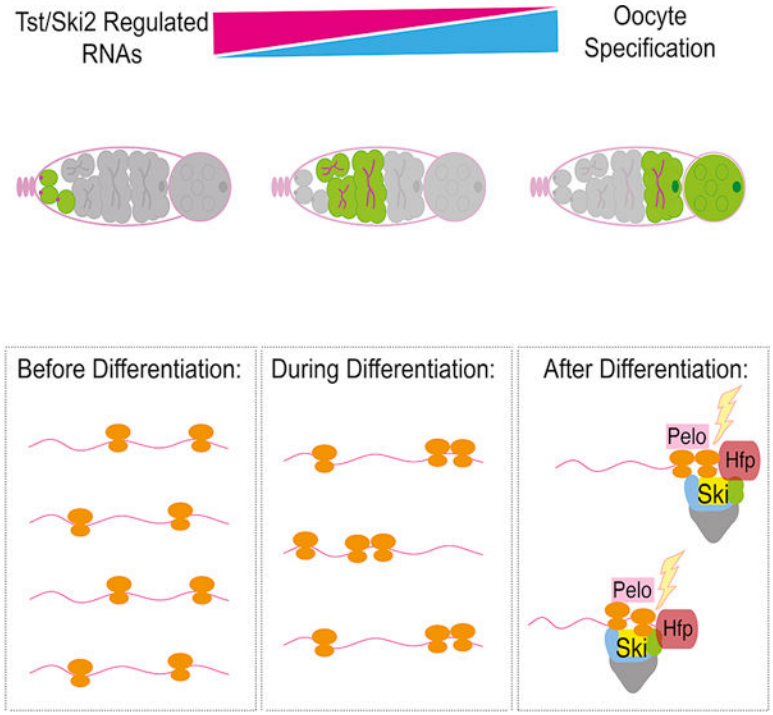

eToc blurb:

Blatt et al. find that a cohort of RNAs expressed in germ cells are targeted for regulated degradation mediated by components of the No Go Decay pathway when oocytes are specified. They find that this regulated RNA degradation is essential for proper oocyte development and fertility.

Introduction

A fertilized egg is totipotent, having the unique potential to differentiate into every cell lineage in the adult organism [1–3]. Across animals, RNA transcribed from 40–75% of all genes is deposited into the egg during oogenesis as a maternal contribution required for embryo development [4–6]. It is unlikely that every RNA synthesized during oogenesis is destined for the maternal contribution – RNAs that support oogenesis-specific functions, such as germline stem cell (GSC) self-renewal and differentiation, could be detrimental during embryogenesis. It is not known if such oogenesis-specific RNAs are targeted for elimination or what, if any, mechanisms ensure that only the appropriate RNAs are contributed to the egg. In *Drosophila*, oogenesis occurs in ovarioles beginning in germaria, which contain the GSCs and the GSC daughter cells (cystoblasts, CBs) that progressively differentiate into 16-cell cysts (Figure 1A–1B) [7–11]. In each cyst, the oocyte enlarges as it receives RNAs and proteins destined to become the maternal contribution from the remaining 15 nurse cells (Figure 1B) [12–18], but the eventual fate of the existing mRNAs that supported oocyte development is unclear.

Results

The Ski complex is required in the female germline for fertility

In a screen to identify novel regulators of oogenesis, we discovered that a component of the RNA-degradation-promoting Super Killer (Ski) complex (Figure 1C), Super Killer 2 (Ski2), called Twister (Tst) in *Drosophila*, is required for egg chamber growth and female fertility (Figure S1A) [19–22]. Wild type (WT) *Drosophila* ovarioles stained for Vasa (germ cells) and for 1B1 (somatic cell membranes) show the progression from the germarium to successively larger egg chambers (Figure 1D). In contrast, egg chambers failed to grow in *tst* mutant ovarioles (Figure 1D–1E, 1N) as well as upon germline RNAi depletion of *tst* (*nanos-GAL4 >*RNAi, Figure 1F–1G, 1N, S1B), but not when *tst* was depleted in the soma (*traffic jam-GAL4 >*RNAi, S1C-S1D) [23,24]. Egg chambers lacking *tst* expressed cleaved Caspase 3 at putative stages 6–7, suggesting that they undergo apoptosis (Figure S1E–S1F). *tst* mutant flies are otherwise viable, and successful oogenesis and viable egg production were restored in *tst* mutants by germline-specific expression of Tst protein (*nanos-GAL4* driver, Figure 1H–1I, 1N, S1A). This maternally expressed *tst* is sufficient to allow for embryonic development, as eggs laid by rescued flies hatched at the same rate as WT control eggs (Figure S1G). Thus, Tst is required in the germline for proper oogenesis.

The Ski complex promotes 3’ to 5’ degradation of mRNAs [20]. In addition to SKI2 (Tst), the Ski complex consists of the scaffolding subunits SKI3 and SKI8, which are coupled to the exosome complex by SKI7 (Figure 1C) [20,21,25,26]. We found that *ski3* (*CG8777*) mutant and germline depletion of *ski3* and *ski8* (*CG3909*) phenocopied *tst* mutants (Figure 1J–1N, S1H–S1J). The conserved GTPase, Hsp70 subfamily B Suppressor (HBS1), is thought to fulfill the role of SKI7 in *Drosophila*; however, female *hbs1* mutants were previously found to be fertile, suggesting that SKI7/HBS1 is dispensable for Ski complex function in the female germline or acts redundantly with a yet-unidentified protein [27–29].

Defects in other mRNA degradation pathways do not elicit the same phenotype as loss of the Ski complex. Loss of exosome components that are required for either nuclear RNA degradation alone (*rRNA-processing 6* (*rrp6*) and *mRNA transport 4* (*mtr4*)) or both nuclear and cytoplasmic RNA degradation (*chromosome disjunction 3* (*dis3*) and *rrp40*) resulted in earlier, germarium-stage defects and complete loss of the germline (Figure S1K–S1R). Defects to the cytoplasmic 5’ mRNA degradation pathway due to loss of *xrn1* still produce late-stage egg chambers, though flies have reduced fecundity [30]. Thus, we conclude that the cytoplasmic 3’ mRNA degradation-promoting Ski complex is required specifically in the fly germ line for egg chamber growth and successful completion of oogenesis.

The Ski complex promotes degradation of a cohort of RNAs during oogenesis

Given the role of the Ski complex in exosome-mediated RNA degradation, we hypothesized that Tst promotes degradation of RNAs during oogenesis [21,31,32]. We performed RNA sequencing (RNA-seq) on ovaries of *tst* mutants and germline RNAi knockdown of *tst* and compared these samples to adult WT ovaries as well as ovaries from virgin flies (young WT) (Figure S2A–S2C). *tst* ovaries are both temporally and morphologically further developed than young WT ovaries, which contain only 2–3 early-stage egg chambers, compared to 6–7

egg chambers in *tst* ovarioles and up to 9–10 chambers in adult WT (Figure S2A–S2C) (see methods). RNA-seq indeed revealed that the *tst* ovary transcriptome closely resembles adult WT (Figure S2A); however, 296 genes are upregulated in ovaries lacking *tst* (Data S1A–B). Among these, 207 genes displayed >4-fold higher levels in germline *tst RNAi* compared to adult WT and are >2-fold upregulated in *tst* genomic mutant ovaries, including *blanks* and *actin57B* (*act57B*) (Figure 2A–2B). These genes likely encode transcripts strongly regulated by Tst in the germline.

We considered whether the elevated levels of genes in *tst* samples could arise from the morphological differences between *tst* ovaries and adult WT, i.e. developmental arrest and loss of late-stage egg chambers that could enrich the *tst* RNA-seq samples for early-stage RNAs. Using previous published single-cell RNA sequencing (scRNA-seq) data from *Drosophila* ovaries [33], we were able to identify 18 genes specifically expressed during early oogenesis that would be expected to be over-represented in bulk RNA-seq samples that are enriched in early-stage egg chambers. However, only 1 out of 18 is >4-fold elevated in *tst RNAi* samples (*rps10a)*, while genes such as *vas*, *bam*, and *cona* are not (Figure S2D). Conversely, maternal mRNAs that would be enriched in egg chambers such as *polar granule component* (*pgc*) and *germ cell-less* (*gcl*) are not decreased in *tst* ovaries compared to adult WT (Figure S2E, Data S1A–B). Thus, the transcriptome differences in *tst* ovaries are not simply due to morphological or developmental differences, and rather reflect specific regulation of a cohort of early-expressed RNAs during oogenesis.

To determine if the upregulation of Tst-regulated mRNAs is due to a defect in post-transcriptional regulation, we measured pre-mRNA levels of select Tst-regulated RNAs and nontargets by qRT-PCR and indeed found no significant difference between WT and *tst* germline RNAi flies (Figure S2F, $p>0.05$, Student's t-test). We also determined that the changes of Tst-regulated RNA levels by RNA-seq are not due to changes in poly(A) tail length: by conducting qRT-PCR primed with random hexamers, we found that *act57b*, *act42a*, *act87e*, and *blanks* RNAs are indeed upregulated in *tst* samples (Figure S2G). Taken together, we find that *tst* promotes the post-transcriptional degradation of a distinct group of RNAs during oogenesis.

Ski complex mediated degradation occurs concurrent with oocyte specification

To characterize the timing of Tst-mediated RNA degradation during oogenesis, we profiled the expression of Tst-regulated RNAs in ovaries across an RNA-seq time course of oocyte development. We enriched for GSCs, CBs, and cysts using mutants (see methods) and compared these samples to germaria and early egg chambers (young WT ovaries), late-stage egg chambers (adult WT ovaries), and unfertilized eggs, which represent the maternal contribution [9,11,34–36]. Principal component analysis (PCA) of stage-enriched samples reveals the developmental trajectory of the oocyte transcriptome and places the *tst* mutant and *tst RNAi* transcriptomes close to the adult WT ovaries, far from the undifferentiated stages (Figure S2A). This suggests that Tst acts after GSC differentiation. Indeed, Tst-regulated RNAs decrease after oocyte differentiation in the cyst stages and are nearly absent in the egg ($p < 1e\text{-}215$, Friedman test) (Figure 2C). This is pattern is not observed for non-targets (Figure S2H–S2I). *In situ* hybridization of the Tst-regulated RNAs such as *blank*s,

act57B, *rps10a*, and *dany* demonstrated that these RNAs are present in the undifferentiated cells and early cyst stages but are degraded by the 16-cell cyst stage in WT when the oocyte is fully specified, in contrast to persistence throughout the egg chambers in *tst* germline RNAi (Figure 2D–2M', S2J–S2K). To further validate when Tst-regulated RNAs are degraded, we also probed for proteins encoded by Tst-regulated *blanks* and *actin* RNAs. In WT, both Blanks and nuclear-Actins (detected by C4 staining) were highly expressed in GSCs and CBs but their expression is attenuated in the cysts, when the oocyte is specified. In contrast, upon loss of *tst*, protein expression of Blanks and Actin was expanded to cyst stages (Figure S2L–S2Q) [37,38]. Thus, Tst mediates the degradation of a cohort of RNAs concurrent with oocyte specification.

No Go decay pathway effector Pelota is required for degradation of Ski complex regulated RNAs

To investigate how specific transcripts are targeted by Tst, we considered the contribution of RNA surveillance pathways, which are known to direct RNAs to the Ski complex for degradation [39]. Nonsense mediated decay (NMD) and non-stop decay (NSD) are unlikely to be involved. In contrast to *tst, ski3*, and *ski8* germline RNAi flies, germline mutant clones of the NMD pathway components *up-frameshift 1* (*Upf1*), *Upf2*, and *Upf3* do produce eggs, albeit with patterning defects [40]. We additionally looked for features in the RNAs that could trigger NMD or NSD. Most Tst-regulated RNAs do not encode introns in their 3' untranslated regions (3' UTR) (Figure S3A), nor show any evidence for aberrant splicing that would give rise to premature termination codons (Figure S3B), ruling out NMD [41–43]. NSD is triggered by ribosome read through into the 3' UTR, but all Tst-regulated mRNAs are annotated transcripts that encode stop codons, suggesting that NSD is unlikely to be involved [44–46].

However, we did find evidence that no-go decay (NGD), which is activated when ribosomes stall on RNAs, was involved in the degradation of Tst-regulated RNAs. Pelota (Pelo/DOM34) is the critical effector protein of the NGD pathway that promotes recycling of stalled ribosomes on mRNAs [27,47,48]. Intriguingly, *pelo* mutants, like *tst* mutants, are homozygous viable but female sterile, and this role is germline specific [49]. *pelo* mutant egg chambers failed to grow and died mid-oogenesis, phenocopying *tst* mutant ovaries (Figure 3A–3C, S3C–S3E'). In addition, *pelo* mutants also lost GSCs, as previously described (Figure S3F–S3G) [49]. To test if *pelo* and *tst* co-regulate target RNAs, we performed RNA-seq on *pelo* mutant ovaries and found that 75% of genes upregulated upon the loss of *tst* were also upregulated >2-fold in *pelo* mutants (156/207, Figure 3D, S2A), including *act57B.* We also find that *blanks* is upregulated 1.9-fold in *pelo* mutants compared to control, just below a 2-fold cut-off. However, *in situ* hybridization for *blanks* RNA in *pelo* mutants showed expanded *blanks* mRNA expression, validating it as a bona fide target (Figure S3H–S3I'). These data suggest that *pelo*, a key component of the NGD pathway, promotes the degradation of a large fraction of Tst-regulated RNAs.

Pelota and Ski complex regulated RNAs exhibit signatures of ribosome stalling

To observe the translation dynamics of Tst-regulated RNAs, we conducted polysome profiling on ovaries enriched for different stages of oocyte development (Figure 3E–3G). We

plotted the expression levels of RNA levels in the polysome RNA fraction (y-axis) compared to the total RNA transcriptome wide (x-axis). In undifferentiated CBs, Tst-regulated RNAs exhibit depressed polysome association (Figure 3E), but overall these RNAs appear to be translated, consistent with detection of Blanks protein in CBs (Figure S3J–S3K'). In differentiating cysts, polysome association of Tst-regulated RNAs increases compared to undifferentiated cells (Figure 3F). However, we did not observe robust Blanks protein in WT cysts (Figure S3K–S3K', S3N), suggesting that ribosome engagement of Tst-regulated RNAs in WT cyst stages is not productive. Finally, in adult WT ovaries, Tst-regulated RNAs recapitulate the low expression we observed previously, but these RNAs exhibit elevated ribosome association as they are degraded (Figure 3G, 3J). In adult WT ovaries, consistent with the absence of *blanks* mRNA, we do not observe Blanks protein expression in the egg chambers (Figure S3K–S3L', S3N).

Increased ribosome association is usually linked to increased RNA stability, but Tst-regulated RNAs showed an increase in ribosome association concomitant with their degradation ($p < 2.2e\text{-}16$, two-way repeated-measures ANOVA) (Figure 3E–G, J), suggesting the presence of stalled ribosomes [50]. As DOM34 (*pelo*) promotes recycling of stalled ribosomes, and SKI2 is required to both extract RNAs from stalled ribosomes and promote their degradation, we predicted that Tst-regulated RNAs would be associated with polysomes, but not degraded in *tst* and *pelo* mutants [51–53]. Indeed, we found that upon loss of *tst* or *pelo*, Tst-regulated RNAs remain highly expressed, associated with ribosomes, and present in egg chambers (Figure 3H–3J). However, in spite of the presence and association of *blanks* RNA with the polysomes, *blanks* RNA is not robustly translated in egg chambers lacking Tst or Pelo (Figure S3K–S3N). Taken together, these results suggest that engagement of ribosomes with Tst-regulated RNAs is unproductive prior to their degradation.

Polypyrimidine tracts are required for degradation Tst-regulated RNAs

Pelo-mediated degradation can be activated by features in the coding sequence that cause ribosome stalling, such as sub-optimal codons [54,55]. We found that Tst-regulated RNAs in fact have an elevated codon optimality compared to non-targets, as measured by the Codon Adaptation Index (CAI), suggesting sub-optimal codon frequency is not the trigger for degradation of Tst-regulated RNAs (Figure S4A) [56,57]. Instead, we identified a motif consisting of repeating, interspaced cytidine residues in the coding sequence (CDS), but not in the 5'UTRs or 3'UTRs, of 60% of Tst-regulated RNAs (124/207, Figure 4A, Data S2A–B), suggesting cytidine tracts might recruit Tst. To investigate this hypothesis, we compared three actin paralogs (*act42A, act57B* and *act87E*), which were upregulated upon the loss of *tst,* to a fourth, *act5C*, which was not upregulated. The *actin* coding sequences are highly similar (>84% nucleotide identity) and have similar CAIs (Figure S4B). A multiple sequence alignment revealed a repeating cytidine tract in the codon wobble position of *act42A, act57B* and *act87E* that is interrupted by purines in the non Tst-target *act5C* (Figure 4B). Disruption of the C-repeat motif correlated with the degree to which the expression of an Actin paralog is affected by loss of Tst: *act57B* with a strong C-repeat motif exhibits high up-regulation in *tst* ovaries compared to *act5C*, which contains purine substitutions and is

unaffected by loss of *tst*, while *act42A* with one purine and one pyrimidine substitution was moderately up-regulated in *tst* ovaries (Figure 4B).

To evaluate the effect of these sequence differences *in vivo*, we built reporters with the GFP open reading frame fused to the CDS of non-target *act5C* or target *act57B*, as well as to a version of *act57B* with cytidine tracts mutated to match *act5C* (PT-mutant). We expressed each of these reporters under the control of the maternal germline promoter *pgc*, as well as the 3'UTR of *K10*, and 5'UTR of *nos* (Figure S4C–S4C''), which are not translationally repressed [34,58–60]. We found no significant change to the levels of either *act5C-GFP* RNA or protein during oocyte specification, or upon loss of *tst* (Figure 4C–4F', 4M–4N, $p>0.05$, two-way ANOVA). In contrast, the levels of both *act57B-GFP* RNA and protein were significantly reduced in WT cysts compared to undifferentiated cells (Figure 4G–4H', 4M–4N, $p<0.001$, two-way ANOVA); we note that the reporter was re-expressed in the egg chambers, which may be due to the strong maternal germline promoter or additional layers of control on Tst-regulated RNAs. Strikingly, upon germline depletion of *tst*, the levels of *act57B-GFP* RNA and protein were strongly elevated in cysts (Figure 4I–4J', 4M–4N). Expression of both RNA and protein from the *act57B PT Mutant-GFP* reporter were significantly higher in cysts compared to that of *act57B-GFP* (Figure 4K–4N, $p<0.001$, two-way ANOVA), matching *act5C-GFP* and demonstrating the importance of the cytidine tract in promoting destabilization of Tst-regulated RNAs during the cyst stages.

To identify the factor that recruits Tst to these cytidine tracts, we looked for polypyrimidine tract binding proteins (PTBs) expressed during oogenesis and found two: *hephaestus* (*heph*) and *half pint* (*hfp*), the homolog of human PUF60. While loss of *heph* does not phenocopy *pelo* and *tst,* loss of *hfp* partially phenocopied the oogenesis defects of *pelo* and *tst*, marked by egg chambers that fail to grow and mid-oogenesis death (Figure 4O–4P, S4D–S4G') [61,62]. Consistent with previous reports, we found that Hfp is present in the nucleus, where it has been shown to regulate splicing, but we also observed it in the cytoplasm, suggesting it could affect RNA stability and translation (Figure S4H–S4I) [62]. To determine if Hfp was bound to Tst-regulated RNAs *in vivo*, we immunoprecipitated Hfp from young WT ovaries followed by qRT-PCR. We found that Tst-regulated RNAs such as *act57B* and *rps10a* were robustly associated with Hfp, whereas non-targets *pgc* and *act5C* were not (Figure S4J). To determine if Hfp also co-regulates Tst-regulated RNAs, we performed RNA-seq of *hfp* mutant ovaries. We found that 71% of the RNAs upregulated in *tst*-depleted ovaries were also upregulated >2-fold in *hfp* mutants, including *act57B, act42A* and *act87E* (148/207, Figure 4Q), whereas *act5C* was not upregulated in either mutant. Furthermore, 59% of Tst-regulated RNAs are upregulated in both *pelo* and *hfp* mutant ovaries, indicating a significant overlap of regulated RNAs between these three factors (Figure S4K, 122/207, $p<9.84e-169$, Hypergeometric test). We did not observe splicing defects of Tst-regulated RNAs in *hfp* mutants, ruling out mis-splicing as the reason for their upregulation (Figure S4L). To determine if Hfp acts in concert with Tst and Pelo, we created a fly carrying GFP-tagged Tst as well as HA-tagged Pelo, which we expressed in the germline with *nosGAL4*. We immunoprecipitated Pelo and probed for Tst and Hfp and found that these proteins interact (Figure S4M). Taken together, our data suggest that Hfp binding to a subset of Tst-regulated RNAs can elicit their degradation mediated by both Pelo and Tst by presumably modulating ribosome association.

Some Ski complex regulated genes are required for germline stem cell maintenance and differentiation, and their ectopic expression perturbs maintenance of oocyte fate

Having elucidated the mechanisms underlying how Tst-regulated RNAs are recognized for degradation, we sought to determine how correct temporal regulation of these RNAs contributes to oogenesis. We hypothesized that Tst-regulated targets are degraded at cyst stages because they have functions prior to or during differentiation and would be detrimental if expressed in the differentiated stages. To determine if there are functional classes of genes in Tst-regulated targets, we carried out gene ontology (GO) analysis and found Tst-regulated targets to be enriched in cytoskeleton components (p=1.03E-05), including *act57B*, *act87E*, and *mlc1*. Actin cytoskeleton is critical during cyst formation and progression [63]. We further assessed the functions of other Tst-regulated RNAs prior to their degradation. Individual depletion of 4 out of 50 Tst-regulated RNAs tested using germline-specific RNAi resulted in severe germline defects, including failure to develop past the germarium stage and complete loss of the germline (Figure S5A–S5E, Table S1). Thus, some Tst-regulated targets have critical function in the undifferentiated stages of oogenesis, though many do not seem to, notably *blanks*, as *blanks* mutant females are fertile [38].

To determine if ectopic expression of Tst-regulated mRNAs can lead to oogenesis defects, we overexpressed *act57B* alone in the germline utilizing *nosGAL4* and a previously characterized UAS-*act57B* [64]. We chose *act57B* as it has previously been reported that overexpression of *act57B* results in female sterility, but the exact nature of the oogenesis defect was not known [64]. We stained ovaries overexpressing *act57B* in the germline and indeed observed egg chamber defects during mid-oogenesis (64%, n=50) (Figure S5F–S5H). Thus, our data suggest that some Tst-regulated targets have a functional role in the undifferentiated cells and need to be removed during oocyte specification to promote oogenesis.

Finally, to elucidate why ectopic persistence of Tst-regulated RNAs interferes with later oogenesis, we examined *tst* mutants for hallmarks of oogenesis defects. We did not find any changes in GSC differentiation or nurse-cell endocycling (Figure S5I–S5N) [11,17,65–68]. However, Egalitarian (Egl), a protein required to transport the maternal RNA contribution to the oocyte, was mislocalized (Figure 5A–5D’). While in WT, Egl always localized to the oocyte and persisted, in *tst, pelo* and *hfp* mutants, Egl localization was not maintained in later egg chambers (Figure 5A–5D’) [13,69]. While initial Egl localization to oocytes appeared to be normal, we cannot rule out subtle specification defects. Taken together, our data suggest that targeted RNA degradation is required for proper establishment of the maternal contribution and maintenance of oocyte fate. Thus, some Tst-regulated RNAs are required in undifferentiated cells for germline maintenance but are detrimental in subsequent stages to the transition to a mature oocyte.

Discussion

In conclusion, we find that specific RNAs expressed during the undifferentiated stages of oogenesis are degraded during oocyte specification, preventing them from being inherited as part of the maternal contribution, and that this turnover is mediated by the Ski complex and the NGD effector Pelo (Figure 5E). Aberrant persistence of these RNAs results in loss of

oocyte maintenance and death of egg chambers. This suggests that precise curation of the maternal contribution is tightly coupled to successful egg production. Based on our observations, we propose that a germ cell-to-maternal transition (GMT) occurs during oocyte specification. We speculate that the GMT exists to enable both the transition from germ cell to oocyte identity and the establishment of the maternal RNA contribution to the embryo. mRNAs produced during oogenesis are subsequently cleared during the oocyte-to-embryo transition (OET) and the maternal-to-zygotic transition (MZT) to promote a zygotic identity [70–72]. Thus, RNA degradation bookends an oocyte's fate, regulating both its inception and termination.

STAR Methods

RESOURCE AVAILABILITY

Lead contact—Further information and requests for resources and reagents should be directed to and will be fulfilled by the lead contact, Prashanth Rangan (Prangan@albany.edu).

Materials availability—Plasmids and transgenic flies generated during this study are maintained in our lab and available upon request.

Data and code availability—All RNA-Sequencing data generated during this study is available in the GEO repository under the Accession number: GSE166275. This study did not generate any code.

EXPERIMENTAL MODEL AND SUBJECT DETAILS

Female *Drosophila melanogaster* flies were maintained in group housing at 25°C and utilized for these studies. Flies were grown at 25°C, fattened overnight on yeast, and dissected between 1–3 days post-eclosion. To achieve stage 9–10 ovarioles, adult WT flies were fattened on yeast overnight for 12–14 hrs.

Genotypes used to enrich specific stages of germline: Germline Stem Cells: *nosGAL4>UAS-tkv* [9,34,73]. Cystoblasts: *nosGAL4>bam RNAi* [11,65,66]. Differentiating Cysts: *nosGAL4>bam RNAi; hs-bam* [35,74]. Female flies were heat shocked at 37° C for 2 hours, incubated at room temperature for 4 hours and heat shocked again for 2 hours. This was subsequently repeated the next day and flies were dissected. Young Wild Type: Female flies were collected and dissected within 2 hours of eclosion.

METHODS DETAILS

Dissection and Immunostaining—Flies were dissected in 1X PBS and samples were fixed for 10 minutes in 5% methanol-free formaldehyde [34]. Ovary samples were washed in 1 mL PBT (1X PBS, 0.5% Triton X-100, 0.3% BSA) 4 times for 7 minutes each. Primary antibodies were added in PBT and incubated at 4°C rotating overnight. Samples were washed 4 times for 7 minutes each in 1 mL PBT, and once in 1 mL PBT with 2% donkey serum for 15 minutes. Secondary antibodies were added in PBT with 4% donkey serum and incubated at room temperature for 2 hours. Samples were washed 4 times for 7 minutes each

in 1 mL of 1X PBST (0.2% Tween 20 in 1x PBS) and incubated in Vectashield with DAPI for 30 minutes before mounting. The following primary antibodies were used: Mouse anti-1B1 (1:20), Rabbit anti-Vasa (1:1000), Chicken anti-Vasa (1:1000), Rabbit anti-GFP (1:2000), Rabbit anti-Blanks (1:1000), Mouse anti-Actin C4 (1:50), Rabbit anti-Cleaved Caspase3 (1:300), Rabbit anti-Egl (1:1000), Mouse anti-Hfp (1:25) [37,75–77]. The following secondary antibodies were used: Alexa 488, Cy3, and Cy5 were used at a dilution of 1:500.

Fluorescence Imaging—The ovary tissue samples were visualized under 10X dry, 20X dry and 40X oil objective lenses and images were acquired using a Zeiss LSM-710 confocal microscope. Confocal images were processed with ImageJ. A.U. The images were quantified using ImageJ with the Measurement function.

Generation of Transgenic Flies—The pCasper2 plasmid containing the *pgc* promoter, *nos* 5'UTR, eGFP CDS and K10 3'UTR was used as a backbone to generate Actin-GFP reporter constructs (Table S2) [34]. gBlocks (IDT) of the *actin5C*, *actin57B* and *actin57B* PT-Mutant CDSs were individually cloned upstream of GFP by digesting with SpeI. Constructs were ligated through Gibson Assembly, utilizing complementary overhangs between the CDS fragment and the pCasper2 backbone. Plasmid was then transformed into DH5α competent cells and plated on LB-Kan plates at 37°C overnight. Cells of individual colonies were propagated, and plasmid was purified. Injection of these plasmids into *Drosophila* embryos was conducted by BestGene Inc.

Gateway Cloning—The complete coding sequence of Tst was PCR amplified from cDNA to include flanking attB sites. BP recombination was carried out according to the manufacturer's protocol using equimolar amounts (100 fmol) of the attB-PCR product and the pDONR entry clone plasmid (Table S2). Components were incubated in TE buffer with BP Clonase enzyme mix and reaction buffer at 25°C for one hour. 2 μg/μL Proteinase K was added to the reaction and incubated at 37°C for one hour. Plasmid was then transformed into DH5α competent cells and plated on LB-Kan plates at 37°C overnight. Cells of individual colonies were propagated, and plasmid was purified. LR recombination reaction was performed with the pPPW and pPGW destination vectors. Components were incubated in TE buffer with LR Clonase enzyme mix and reaction buffer at 25°C for one hour. 2 μg/μL Proteinase K was added to the reaction and incubated at 37°C for one hour. Plasmid was then transformed into XL10-Gold competent cells and plated on LB-Kan plates at 37°C overnight. Cells of individual colony samples were propagated, plasmid was purified and sequenced to verify insertion.

RNA Isolation and cDNA Synthesis—Ovaries were dissected in 1X PBS and homogenized in 50uL of TRIzol [34]. RNA was isolated by adding an additional 950 uL of TRIzol and 230uL of Chloroform with mixing. Samples were centrifuged at 13,000 rpm, 4°C for 15 minutes. Aqueous phase was transferred to a new tube, nucleic acids were precipitated using 1 mL of 100% ethanol, 50 μL of 3M Sodium Acetate and precipitated for >1 hour at −20°C. Samples were centrifuged at 13,000 rpm, 4°C for 20 minutes. Ethanol was decanted, pellet was washed with 70% ethanol and dried at room temperature for 10

minutes. Pellet was dissolved in 20 μL RNase free water and placed in a 42°C water bath for 10 minutes. Concentration of nucleic acid samples were measured on a spectrophotometer and treated with DNase according to the manufacturer's protocol. cDNA was synthesized using SuperScript 2 and according to the manufacturer's protocol. To reverse transcribe mRNAs, Oligo-dT was used from the SuperScript 2 kit. To reverse transcribe nascent pre-mRNAs, or mRNAs independent of poly(A) tail length, 150 ng of random hexamers per sample was used from the SuperScript 2 kit.

Quantitative Real Time-PCR (qRT-PCR)—1 μL of cDNA was amplified using 5μL of SYBR green Master Mix, 0.3 μL of 10μM of each reverse and forward primers in a 10 μL reaction [34]. The thermal cycling conditions consisted of 50°C for 2 minutes, 95°C for 10 minutes, 40 cycles at 95°C for 15 seconds, and 60°C for 60 seconds. The experiments were carried out in technical triplicate and minimum 2 biological replicates for each sample. *rp49* gene was utilized as a control. To calculate fold change in mRNA levels to *rp49* mRNA levels, average of the 2^ΔCt for the biological replicates was calculated. Error bars were plotted using standard error of the ratios. P-value was determined by a two sample Student's t-test.

RNA-seq library preparation—Total RNA samples were run on a 1% agarose gel to assess sample integrity [78]. To generate mRNA-Seq libraries, total RNA was incubated with poly(A) selection beads. mRNA enriched sequencing libraries were made with the NEXTflex Rapid Directional RNAseq Kit and corresponding protocol. mRNA was fragmented at 95°C for 13 minutes to achieve ~300 bp fragments. The WT_1, Young_1, Tst_1 and Tst_RNAi_1 library samples are unstranded and were sequenced by Beijing Genomics Institute on a HiSeq4000. All other Library samples were sequenced with 75 bp single-end or paired-end mRNA by an Illumina NextSeq500, carried out by the Center for Functional Genomics (CFG).

EdU—Ovaries were dissected into Schneider's Media and incubated in 10μM EdU solution rotating for one hour [79]. Samples were fixed in 3.7% formaldehyde in PBS, rotating for 30 minutes. Fixative was then aspirated and samples were washed with 1 mL PBS for 10 minutes and permeabilized in 1 mL of permeabilization solution (1% Triton X-100 in PBST) rotating for 20 minutes. Samples were then washed in 1 mL PBS rotating for 10 minutes. Click-iT reaction cocktail (PBS, $CuSO_4$, Fluorescent dye azide and Reaction Buffer Additive) was made according to manufacturer's directions and added to each sample. Tubes were protected from light and rotated at room temperature for 30 minutes. Samples were then washed once with 1 mL of Click-iT reaction rinse buffer and once with 1 mL PBS. Ovary samples were then transitioned to the immunostaining protocol.

Fluorescent *in situ* Hybridization—Ovaries were dissected in RNase free 1X PBS and fixed in 1 mL of 5% formaldehyde rotating for 10 minutes. Samples were then washed three times for five minutes each in PT buffer (PBS, 0.1% Triton X-100) and dehydrated in successive methanol washes for six minutes each (30%, 50%, 70%). A final 100% methanol wash was carried out for 12 minutes. Samples were equilibrated to PT buffer by conducting successive methanol washes for six minutes each (70%, 50%, 30%), followed by three PT

washes of six minutes each. Ovaries were pre-hybridized for six minutes in 1 mL Wash buffer (10% Deionized Formamide, 2X SSC in RNase Free H_2O). CALFluor590 tagged probes against GFP were used. Hybridization of probes was conducted at 32°C, covered for >16 hours. Samples were then washed six times in Wash buffer for 2 minutes per wash. Samples were then washed twice in 1 mL Wash buffer for 30 minutes at 30°C. Wash buffer was aspirated and incubated in Vectashield for 30 minutes before mounting. *in situ* experiments were repeated more than three times for control and *experimental* ovaries.

RNAScope™ Assay—We utilized a modified RNAscope procedure for *Drosophila* ovaries described previously [80]. Probes were designed and generated by Advanced Cell Diagnostics with specificity to target base pairs 29–1250 of *blanks* mRNA (NCBI accession number: NM_139709.2), base pairs 1196–1693 of *actin57B* mRNA (NM_079076.4), base pairs 213–1141 of *dany* mRNA (NM_166493.2), base pairs 2–599 of *rps10a* mRNA (NM_143319.4). Ovaries were dissected in RNase free 1X PBS and fixed in 1 mL of 5% formaldehyde rotating for 10 minutes. Samples were then washed three times for five minutes each in PT buffer (PBS, 0.1% Triton X-100) and dehydrated in successive methanol washes for six minutes each (30%, 50%, 70%). A final 100% methanol wash was carried out for 12 minutes. Samples were equilibrated to PT buffer by conducting successive methanol washes for six minutes each (70%, 50%, 30%), followed by three PT washes of six minutes each. Ovaries were pre-hybridized for six minutes in 1 mL of RNAScope Wash buffer. Hybridization of probes was conducted at 40°C, covered for >16 hours. Samples were then washed three times in RNAscope wash buffer for 5 minutes per wash, fixed in 4% formaldehyde in 1X PBS at room temperature for 10 minutes and washed in buffer three times for 5 minutes each. Ovaries were incubated in a successive series of amplifier solutions (Amp). Amp 1 for at least 45 minutes at 40°C, Amp 2 for 45 minutes at 40°C, Amp 3 for 45 minutes at 40°C, Amp 4 for 45 minutes at 40°C. After each Amp step ovaries were washed in wash buffer 5 times for 3 minutes each at room temperature. Samples were then washed in 1 mL PBT for 5 minutes and mounted in Vectashield. RNAscope experiments were repeated more than three times for control and, *pelo*, and *tst RNAi* ovaries.

Materials and reagents—Fly food was made according to previously published procedures, and filled narrow vials to approximately 12mL [34].

Immuno-Precipitation (IP) and RNA Immuno-Precipitation (RIP)—65 pairs of ovaries were dissected in 1X PBS [34]. After dissection, PBS was aspirated and 100 µl of RIPA buffer (50 mM Tris pH 8.0, 1% Triton X-100, 0.1% sodium deoxycholate, 0.1% SDS, 140 mM NaCl, 1mM EDTA, 1 mM PMSF, 1 protease inhibitor pill per 50 ml) was added and the sample was homogenized. An additional 200 µl of RIPA buffer was added to the lysate and mixed. The lysate was then centrifuged at 13,000 rpm for 10 minutes at 4°C. The supernatant was transferred to a new tube. 10% of the cleared homogenate was set aside as input, 4X SDS buffer was added the sample was heated at 95°C for 5 minutes and stored at −20°C until Western analysis. An additional 10% of homogenate was used for RNA input, 100 µl of TriZol was added, mixed and this sample was stored in −80°C. 40% of homogenate was used for the IgG control and the remaining 40% was used for RIP. The following antibody was added to the lysate and incubated at 4°C for 3 hours; 1 µl of Rabbit

anti-HA. Protein A Dynabeads were separated into 15 μl aliquots for each sample and washed four times in 400 μl of 1:10 diluted protease inhibitor-containing Net2 buffer (50 mM Tris-Cl [pH 8.0], 150 mM NaCl, 10% NP-40) on a magnetic rack. The beads were then re-suspended in 100 μl of Net2 buffer. After lysate incubation 25 μl of washed beads was added to each sample and incubated overnight at 4°C. Beads were washed six times with 500 μl of 1:10 diluted Net2 buffer for 2 minutes each. Beads were then resuspended in 25 μl of Net2 buffer. An aliquot of 10 μl was used for Western Blot analysis. The remaining 15 μl was used for RNA extraction.

Subcellular Fractionation—50 adult Wild Type ovaries were dissected in 1X PBS and gently homogenized with 10–20 strokes of a plastic homogenizer in 100 μL hypotonic lysis buffer (10mM HEPES pH 7.9, 1.5 mM $MgCl_2$, 10 mM KCl, 0.5 mM DTT). Homogenate was incubated on ice for 15 minutes. 50 μL of homogenate was aliquoted in a new tube, 4X SDS buffer was added, sample was boiled at 95°C for 5 minutes and stored in −20°C until use as total homogenate. The remaining homogenate was centrifuged for 10 minutes at 1000g. 50 μL of supernatant was collected 4X SDS buffer was added, sample was boiled at 95°C for 5 minutes and stored in −20°C until use as cytoplasmic fraction. The pellet was resuspended in high salt extraction buffer (20mM HEPES pH 7.9, 25% glycerol, 420 mM NaCl, 1.5 mM $MgCl_2$, 0.2 mM EDTA, 0.5 mM DTT) and centrifuged for 5 minutes at 20,000g. Supernatant was collected 4X SDS buffer was added, sample was boiled at 95°C for 5 minutes and stored in −20°C until use as total nuclear fraction.

Western Blot—Twenty wild-type size ovaries or 40 mutant size ovaries were dissected in 1X PBS [34]. After dissection, PBS was aspirated and 30 μl of NP-40 buffer with protease inhibitors added to the tissue and homogenized. The lysate was centrifuged at 13,000 rpm for 15 minutes at 4°C. Aqueous layer was transferred into a new tube while avoiding the top lipid layer. 1 μl of the protein extract was used to carry out a Bradford assay. 25 μg of protein was denatured with 4X Laemmli Sample Buffer and β-marcepthanol at 95°C for 5 minutes. The samples were loaded in a Mini-PROTEAN TGX 4–20% gradient SDS-PAGE gels and run at 110V for 1 hour. The proteins were then transferred to a 0.20 μm nitrocellulose membrane at 100V for 1 hour at 4°C. After transfer, the membrane was blocked in 5% milk in PBST for 2 hours at RT. The following antibodies were used: Mouse anti-Hfp (1:1000), Rabbit anti-Orb (1:1000), Mouse anti-Fibrillarin (1:25), Rabbit anti-HA (1:1000), Rabbit anti-GFP (1:1000). Primary antibody was prepared in 5% milk in PBST was added to the membrane and incubated at 4°C overnight. The membrane was then washed three times in 0.5% milk PBST. Anti-Rabbit HRP (1:10,000) or Anti-Mouse HRP (1:10,000) was prepared in 5% milk in PBST, and was added to the membrane and incubated at room temperature for 2 hours. The membrane was then washed 3 times in PBST. Bio-rad chemiluminescence ECL kit was used to image the membrane.

Egg Laying Test and Viability Assay—Newly eclosed flies were collected and fattened overnight on yeast. Assays were conducted in cages on apple juice plates containing 6 control or experimental females crossed to 4 adult Wild Type control males. Cages were maintained at 25°C and plates changed daily for egg counting. Analyses were performed on three consecutive days. Total number of eggs laid was counted and averaged. For viability

assays, hatched larvae were counted 48 hours later and were assessed as a proportion of eggs hatched/eggs laid. Both control and experimental experiments were conducted in triplicate.

Polysome profiling and Polysome-Seq—30 Wild Type or 150 mutant ovary pairs were dissected in 1X PBS and immediately flash frozen on liquid nitrogen [34,81]. Samples were homogenized in lysis buffer and 20% of lysate was used as input for mRNA isolation and library preparation (as described above). Samples were loaded onto 10–45% CHX supplemented sucrose gradients in 9/16 × 3.5 PA tubes (Beckman Coulter, #331372). For samples used for protein isolation, 650 μg/mL of heparin was added to sucrose gradients. Gradients were spun at 35,000 x g in SW41 for 3 hours at 4°C. Gradients were fractionated with a Density Gradient Fractionation System (#621140007). RNA was extracted using acid phenol-chloroform and precipitated overnight. Pelleted RNA was resuspended in 20 μL water, treated with TURBO DNase and libraries were prepared as described above. For samples used for protein isolation, 4 volumes of methanol was added to each fraction and centrifuged at 13,000g for 5 minutes. Methanol was aspirated and pellet was dried before being resuspended in 1X Laemli SDS buffer.

MEME Analyses—The 5'UTR, CDS, 3'UTR and full transcript sequences of all 207 Tst-regulated target genes were individually analyzed by the MEME algorithm [82]. Discriminative mode analysis was conducted against 621 non-target gene sequences as background with default parameters. FIMO was conducted by entering a repeating "CNN" motif and conducting a search for this motif in the *blanks* CDS [83]. Motif logos, number of sites, and p-values all reported as produced by output of the program.

QUANTIFICATION AND STATISTICAL ANALYSIS

RNA-seq analysis—Sequenced reads were aligned to the *D. melanogaster* genome (UCSC dm6 and FlyBase R6.01) using HISAT2 v2.0.5 [84]. Unambiguously mapping reads to RefSeq annotated mRNA and lincRNA were quantified using featureCounts v1.5.1 default parameters [85]. Genes with>=0.5 reads per million (RPM) in one of WT ovaries, *tst* mutant ovaries, *tst RNAi* ovaries, or young ovaries were retained for further analysis (N=9251 genes). Tst regulated mRNAs were classified as genes whose transcript-per-million (TPM) expression levels were >4-fold increased in the *tst RNAi* samples; a subset of these that are additionally >2-fold increased in the *tst* mutant samples were considered to be strong Tst regulated mRNAs (N=207 genes). DESeq2 was subsequently used to confirm significance of these targets (Data S1C–D)[86]. To curate a set of non-target genes to serve as a background set, we identified genes that differed <1.25 fold between WT and *tst RNAi* and selected the 3 non-targets with the most similar *tst RNAi* expression level to each Tst regulated mRNA, to yield a set of 621 non-targets. For polysome profiling samples, normalized ribosome occupancy was calculated as $\log_2$(polysome TPM / input TPM). A 0.5 pseudocount was added to each TPM value to prevent division by zero and taking the log of zero. To compare ribosome occupancy of Tst regulated mRNAs across different conditions relative to the global differences observed, we normalized Tst regulated mRNA ribosome occupancy by mean non-target occupancy, i.e. $\log_2$((polysome_target TPM / input_target TPM) / average (polysome_non-target TPM / input_non-target TPM)). Codon optimality index (CAI) was calculated for each gene relative to the codon frequencies in the top 100

expressed genes in WT ovaries according to the method of Sharp & Li, 1987 [56]. To measure Tst-target expression change over the developmental timecourse, we performed a Friedman test (non-parametric one-way ANOVA with repeated measures). Individual post-hoc tests between stages were performed using Wilcoxon signed rank tests with Bonferonni correction for (8 choose 2) = 28 comparisons. To measure changes in ribosome occupancy in the polysome profiling data, we performed a two-way repeated measures ANOVA modeling, per gene, the difference in ribosome occupancy ($\log_2$ polysome TPM / input TPM) versus classification as Twister target or non-target (occupancy ~ condition * target_type) using the lme function in the R package nlme (v3.1–149, Pinheiro & Bates). P value is from a likelihood test against a null model (occupancy ~ 1). Post-hoc tests between conditions given target type were performed using the R package emmeans (v1.5.2–1, Lenth et al). All RNA-Seq data utilized in this work are summarized in Data S1A–D, and raw reads are available under the following GEO accessions: GSE119458, GSE143728, and GSE166275.

Statistical Analyses—All statistical analyses were conducted in Excel or R as noted. The specific tests, sample, size, p-value and asterisks are displayed in the corresponding legends.

Supplementary Material

Refer to Web version on PubMed Central for supplementary material.

Acknowledgements

We would like to thank all members of the Rangan Lab as well as Drs. Siekhaus D, Sano H, Juliano C, Belfort M, and Farrell J for discussion and comments on the manuscript. We would also like to thank the Schüpbach Lab for the Hfp antibody and mutant flies, the Sontheimer Lab for the Blanks antibody, and the Newbury Lab for flies and reagents. P.R. is funded by the NIH/NIGMS (R01GM111779–06 and R01GM135628–01). P.B. is funded by NIH (grant 1F31GM126784–01) and by the RNA Institute. M.T.L. was supported by the NIH/NIGMS (R35GM135099) and start-up funds from the Univ. of Pittsburgh.

References

[1]. Cinalli RM, Rangan P, Lehmann R. Germ cells are forever. Cell 2008;132:559–62. doi:10.1016/j.cell.2008.02.003. [PubMed: 18295574]

[2]. Seydoux G, Braun RE. Pathway to Totipotency: Lessons from Germ Cells. Cell 2006;127:891–904. doi:10.1016/j.cell.2006.11.016. [PubMed: 17129777]

[3]. Reik W, Surani MA. Germline and Pluripotent Stem Cells. Cold Spring Harbor Perspectives in Biology 2015;7.

[4]. Walser CB, Lipshitz HD. Transcript clearance during the maternal-to-zygotic transition. Current Opinion in Genetics & Development 2011;21:431–43. doi:10.1016/j.gde.2011.03.003. [PubMed: 21497081]

[5]. Laver JD, Marsolais AJ, Smibert CA, Lipshitz HD. Regulation and Function of Maternal Gene Products During the Maternal-to-Zygotic Transition in Drosophila. Current Topics in Developmental Biology 2015;113:43–84. doi:10.1016/bs.ctdb.2015.06.007. [PubMed: 26358870]

[6]. Lee MT, Bonneau AR, Giraldez AJ. Zygotic Genome Activation During the Maternal-to-Zygotic Transition. Annu Rev Cell Dev Biol 2014;30:581–613. doi:10.1146/annurev-cellbio-100913-013027. [PubMed: 25150012]

[7]. Lehmann R Germline stem cells: Origin and destiny. Cell Stem Cell 2012;10:729–39. doi:10.1016/j.stem.2012.05.016. [PubMed: 22704513]

[8]. Spradling AC, de Cuevas M, Drummond-Barbosa D, Keyes L, Lilly M, Pepling M, et al. The Drosophila germarium: stem cells, germ line cysts, and oocytes. Cold Spring Harbor Symposia on Quantitative Biology 1997;62:25–34. [PubMed: 9598333]

[9]. Xie T, Spradling AC. decapentaplegic is essential for the maintenance and division of germline stem cells in the Drosophila ovary. Cell 1998;94:251–60. doi:10.1016/s0092-8674(00)81424-5. [PubMed: 9695953]

[10]. Spradling A, Drummond-Barbosa D, Kai T. Stem cells find their niche. Nature 2001;414:98–104. [PubMed: 11689954]

[11]. McKearin DM, Spradling AC. bag-of-marbles: a Drosophila gene required to initiate both male and female gametogenesis. Genes & Development 1990;4:2242–51. doi:10.1101/gad.4.12b.2242. [PubMed: 2279698]

[12]. Eichhorn SW, Subtelny AO, Kronja I, Kwasnieski JC, Orr-Weaver TL, Bartel DP. mRNA poly(A)-tail changes specified by deadenylation broadly reshape translation in Drosophila oocytes and early embryos. eLife 2016;5:1–24. doi:10.7554/eLife.16955.

[13]. Navarro C, Puthalakath H, Adams JM, Strasser A, Lehmann R. Egalitarian binds dynein light chain to establish oocyte polarity and maintain oocyte fate. Nat Cell Biol 2004;6:427–35. doi:10.1038/ncb1122. [PubMed: 15077115]

[14]. Huynh J-R, St Johnston D. The origin of asymmetry: early polarisation of the Drosophila germline cyst and oocyte. Current Biology 2004;14:R438–49. [PubMed: 15182695]

[15]. Lantz V, Chang JS, Horabin JI, Bopp D, Schedl P. The Drosophila orb RNA-binding protein is required for the formation of the egg chamber and establishment of polarity. Genes & Development 1994;8:598–613. doi:10.1101/gad.8.5.598. [PubMed: 7523244]

[16]. Kugler J-M, Lasko P. Localization, anchoring and translational control of oskar, gurken, bicoid and nanos mRNA during drosophila oogenesis. Fly 2009;3:15–28. doi:10.4161/fly.3.1.7751. [PubMed: 19182536]

[17]. Spradling AC, Mahowald AP. Amplification of genes for chorion proteins during oogenesis in <em>Drosophila melanogaster</em&gt. Proc Natl Acad Sci USA 1980;77:1096. [PubMed: 6767241]

[18]. Navarro-Costa P, McCarthy A, Prudêncio P, Greer C, Guilgur LG, Becker JD, et al. Early programming of the oocyte epigenome temporally controls late prophase i transcription and chromatin remodelling. Nat Comms 2016;7. doi:10.1038/ncomms12331.

[19]. Seago JE, Chernukhin IV, Newbury SF. The Drosophila gene twister, an orthologue of the yeast helicase SKI2, is differentially expressed during development. Mechanisms of Development 2001;106:137–41. doi:10.1016/S0925-4773(01)00429-4. [PubMed: 11472843]

[20]. Anderson JS, Parker RP. The 39 to 59 degradation of yeast mRNAs is a general mechanism for mRNA turnover that requires the SKI2 DEVH box protein and 39 to 59 exonucleases of the exosome complex. Embo J 1998;17:1497–506. [PubMed: 9482746]

[21]. Halbach F, Rode M, Conti E. The crystal structure of S. cerevisiae Ski2, a DExH helicase associated with the cytoplasmic functions of the exosome. Rna 2012;18:124–34. doi:10.1261/rna.029553.111. [PubMed: 22114319]

[22]. Schmidt C, Kowalinski E, Shanmuganathan V, Defenouillere Q, Braunger K, Heuer A, et al. The cryo-EM structure of a ribosome–Ski2-Ski3-Ski8 helicase complex. Science 2016;354:1431–3. doi:10.1126/science.aaf7520. [PubMed: 27980209]

[23]. Tanentzapf G, Devenport D, Godt D, Brown NH. Integrin-dependent anchoring of a stem-cell niche. Nat Cell Biol 2007;9:1413–8. [PubMed: 17982446]

[24]. Doren MV, Williamson AL, Lehmann R. Regulation of zygotic gene expression in Drosophila primordial germ cells. Current Biology 1998;8:243–6. doi:10.1016/S0960-9822(98)70091-0. [PubMed: 9501989]

[25]. Halbach F, Reichelt P, Rode M, Conti E. The Yeast Ski Complex: Crystal Structure and RNA Channeling to the Exosome Complex. Cell 2013;154:814–26. doi:10.1016/j.cell.2013.07.017. [PubMed: 23953113]

[26]. Théry C, Zitvogel L, Amigorena S. Exosomes: composition, biogenesis and function. Nat Rev Immunol 2002;2:569–79. doi:10.1038/nri855. [PubMed: 12154376]

[27]. Becker T, Armache J-P, Jarasch A, Anger AM, Villa E, Sieber H, et al. Structure of the no-go mRNA decay complex Dom34-Hbs1 bound to a stalled 80S ribosome. Nat Struct Mol Biol 2011;18:715–20. doi:10.1038/nsmb.2057. [PubMed: 21623367]

[28]. Yang F, Zhao R, Fang X, Huang H, Xuan Y, Ma Y, et al. The RNA surveillance complex Pelo-Hbs1 is required for transposon silencing in the Drosophila germline. EMBO Reports 2015;16:965–74. doi:10.15252/embr.201540084. [PubMed: 26124316]

[29]. Li Z, Yang F, Xuan Y, Xi R, Zhao R. Pelota-interacting G protein Hbs1 is required for spermatogenesis in Drosophila. Sci Rep 2019:1–14. doi:10.1038/s41598-019-39530-6. [PubMed: 30626917]

[30]. Nagarajan VK, Jones CI, Newbury SF, Green PJ. XRN 5′→3′ exoribonucleases: Structure, mechanisms and functions. Biochimica Et Biophysica Acta (BBA) - Gene Regulatory Mechanisms 2013;1829:590–603. doi:10.1016/j.bbagrm.2013.03.005. [PubMed: 23517755]

[31]. Théry C, Zitvogel L, Amigorena S. Exosomes: composition, biogenesis and function. arXiv 2002;2:569–79. doi:10.1038/nri855.

[32]. Halbach F. Structural and Functional Characterization of the Yeast Ski2-Ski3-Ski8 Complex 2013:1–126.

[33]. Jevitt A, Chatterjee D, Xie G, Wang X-F, Otwell T, Huang Y-C, et al. A single-cell atlas of adult Drosophila ovary identifies transcriptional programs and somatic cell lineage regulating oogenesis. PLoS Biol 2020;18:e3000538. doi:10.1371/journal.pbio.3000538. [PubMed: 32339165]

[34]. Flora P, Wong-Deyrup SW, Martin ET, Palumbo RJ, Nasrallah M, Oligney A, et al. Sequential Regulation of Maternal mRNAs through a Conserved cis-Acting Element in Their 3' UTRs. CellReports 2018;25:3828–9.

[35]. Ohlstein B, McKearin D. Ectopic expression of the Drosophila Bam protein eliminates oogenic germline stem cells. Development 1997;124:3651. [PubMed: 9342057]

[36]. Jia Ng SS, Zheng RT, Osman I, Pek JW. Generation of Drosophila sisRNAs by Independent Transcription from Cognate Introns. Iscience 2018;4:68–75. [PubMed: 30240754]

[37]. Kelpsch DJ, Groen CM, Fagan TN, Sudhir S, Tootle TL. Fascin regulates nuclear actin during Drosophila oogenesis. Molecular Biology of the Cell 2016;27:2965–79. doi:10.1091/mbc.E15-09-0634. [PubMed: 27535426]

[38]. Gerbasi VR, Preall JB, Golden DE, Powell DW, Cummins TD, Sontheimer EJ. Blanks, a nuclear siRNA/dsRNA-binding complex component, is required for Drosophila spermiogenesis. Pnas 2011;108:3204–9. doi:10.1073/pnas.1009781108/-/DCSupplemental. [PubMed: 21300896]

[39]. Schneider C, Tollervey D. Threading the barrel of the RNA exosome 2013:1–9. doi:10.1016/j.tibs.2013.06.013.

[40]. Avery P, Vicente-Crespo M, Francis D, Nashchekina O, Alonso CR, Palacios IM. Drosophila Upf1 and Upf2 loss of function inhibits cell growth and causes animal death in a Upf3-independent manner. Rna 2011;17:624–38. doi:10.1261/rna.2404211. [PubMed: 21317294]

[41]. Mitchell P, Tollervey D. An NMD pathway in yeast involving accelerated deadenylation and exosome-mediated 3′→5′ degradation. Molecular Cell 2003;11:1405–13. doi:10.1016/S1097-2765(03)00190-4. [PubMed: 12769863]

[42]. Lykke-Andersen S, Jensen TH. Nonsense-mediated mRNA decay: an intricate machinery that shapes transcriptomes. Nature Publishing Group 2015;16:665–77. doi:10.1038/nrm4063.

[43]. Peltz SW, Brown AH, Jacobson A. mRNA destabilization triggered by premature translational termination depends on at least three cis-acting sequence elements and one trans-acting factor. Genes & Development 1993;7:1737–54. doi:10.1101/gad.7.9.1737. [PubMed: 8370523]

[44]. Dunn JG, Foo CK, Belletier NG, Gavis ER, Weissman JS. Ribosome profiling reveals pervasive and regulated stop codon readthrough in Drosophila melanogaster. eLife 2013;2013:1–32. doi:10.7554/eLife.01179.

[45]. Hashimoto Y, Takahashi M, Sakota E, Nakamura Y. Nonstop-mRNA decay machinery is involved in the clearance of mRNA 5′-fragments produced by RNAi and NMD in Drosophila melanogaster cells. Biochemical and Biophysical Research Communications 2017;484:1–7. doi:10.1016/j.bbrc.2017.01.092. [PubMed: 28115162]

[46]. Schweingruber C, Rufener SC, Zünd D, Yamashita A, Mühlemann O. Nonsense-mediated mRNA decay — Mechanisms of substrate mRNA recognition and degradation in mammalian cells. BBA - Gene Regulatory Mechanisms 2013;1829:612–23. [PubMed: 23435113]

[47]. Kobayashi K, Kikuno I, Kuroha K, Saito K, Ito K, Ishitani R, et al. Structural basis for mRNA surveillance by archaeal Pelota and GTP-bound EF1alpha complex. Proc Natl Acad Sci USa 2010;107:17575–9. doi:1009598107 [pii]. [PubMed: 20876129]

[48]. Jamar NH, Kritsiligkou P, Grant CM. The non-stop decay mRNA surveillance pathway is required for oxidative stress tolerance. Nucleic Acids Research 2017;45:6881–93. doi:10.1093/nar/gkx306. [PubMed: 28472342]

[49]. Xi R, Doan C, Liu D, Xie T. Pelota controls self-renewal of germline stem cells by repressing a Bam-independent differentiation pathway. Development 2005;132:5365–74. doi:10.1242/dev.02151. [PubMed: 16280348]

[50]. Edri S, Tuller T. Quantifying the Effect of Ribosomal Density on mRNA Stability. PLoS ONE 2014;9:e102308. doi:10.1371/journal.pone.0102308. [PubMed: 25020060]

[51]. Guydosh NR, Green R. Dom34 Rescues Ribosomes in 3′ Untranslated Regions. Cell 2014;156:950–62. doi:10.1016/j.cell.2014.02.006. [PubMed: 24581494]

[52]. Guydosh NR, Green R. Translation of poly(A) tails leads to precise mRNA cleavage. Rna 2017;23:749–61. doi:10.1261/rna.060418.116. [PubMed: 28193672]

[53]. Zinoviev A, Ayupov RK, Abaeva IS, Hellen CUT, Pestova TV. Extraction of mRNA from Stalled Ribosomes by the Ski Complex. Molecular Cell 2020;77:1340–6. [PubMed: 32006463]

[54]. Simms CL, Yan LL, Zaher HS. Ribosome Collision Is Critical for Quality Control during No-Go Decay. Molecular Cell 2017;68:361–5. doi:10.1016/j.molcel.2017.08.019. [PubMed: 28943311]

[55]. Hanson G, Coller J. Codon optimality, bias and usage in translation and mRNA decay. Nat Rev Mol Cell Biol 2017. doi:10.1038/nrm.2017.91.

[56]. Sharp PM, Li WH. The codon Adaptation Index--a measure of directional synonymous codon usage bias, and its potential applications. Nucleic Acids Research 1987;15:1281–95. [PubMed: 3547335]

[57]. Presnyak V, Alhusaini N, Chen Y-H, Martin S, Morris N, Kline N, et al. Codon optimality is a major determinant of mRNA stability. Cell 2015;160:1111–24. doi:10.1016/j.cell.2015.02.029. [PubMed: 25768907]

[58]. Serano TL, Cheung H-K, Frank LH, Cohen RS. P element transformation vectors for studying Drosophila melanogaster oogenesis and early embryogenesis. Gene 1994;138:181–6. [PubMed: 8125300]

[59]. Gavis ER, Lehmann R. Localization of nanos RNA controls embryonic polarity. Cell 1992;71:301–13. doi:10.1016/0092-8674(92)90358-j. [PubMed: 1423595]

[60]. Gavis ER, Lehmann R. Translational regulation of nanos by RNA localization. Nature 1994;369:315–8. doi:10.1038/369315a0. [PubMed: 7514276]

[61]. McDermott SM, Davis I. Drosophila Hephaestus/polypyrimidine tract binding protein is required for dorso-ventral patterning and regulation of signalling between the germline and soma. PLoS ONE 2013;8:e69978–8. [PubMed: 23894566]

[62]. Van Buskirk C, Trudi S. Half pint Regulates Alternative Splice Site Selection in Drosophila 2002:1–11.

[63]. Chanet S, Huynh J-R. Collective Cell Sorting Requires Contractile Cortical Waves in Germline Cells. Current Biology 2020;30:4213–4. [PubMed: 32916115]

[64]. Roper K Contribution of sequence variation in Drosophila actins to their incorporation into actin-based structures in vivo. Journal of Cell Science 2005;118:3937–48. doi:10.1242/jcs.02517. [PubMed: 16105877]

[65]. Chen D, McKearin D. Dpp signaling silences bam transcription directly to establish asymmetric divisions of germline stem cells. Current Biology 2003;13:1786–91. doi:10.1016/j.cub.2003.09.033. [PubMed: 14561403]

[66]. Chen D, Mckearin DM. A discrete transcriptional silencer in the bam gene determines asymmetric division of the Drosophila germline stem cell. Development (Cambridge, England) 2003;130:1159–70. doi:10.1242/dev.00325.

[67]. Lilly MA, Sptadling AC. The Drosophila endocycle is controlled by cyclin E and lacks a checkpoint ensuring S-phase completion. Genes & Development 1996;10:2514–26. doi:10.1101/gad.10.19.2514. [PubMed: 8843202]

[68]. Calvi BR, Lilly MA, Spradling AC. Cell cycle control of chorion gene amplification. Genes & Development 1998;12:734–44. [PubMed: 9499407]

[69]. Mach JM, Lehmann R. An Egalitarian-BicaudalD complex is essential for oocyte specification and axis determination in Drosophila. Genes & Development 1997;11:423–35. doi:10.1101/gad.11.4.423. [PubMed: 9042857]

[70]. Schultz RM. The molecular foundations of the maternal to zygotic transition in the preimplantation embryo. Hum Reprod Update 2002;8:323–31. doi:10.1093/humupd/8.4.323. [PubMed: 12206467]

[71]. Tadros W, Houston SA, Bashirullah A, Cooperstock RL, Semotok JL, Reed BH, et al. Regulation of maternal transcript destabilization during egg activation in Drosophila. Genetics 2003;164:989–1001. [PubMed: 12871909]

[72]. Cabrera Quio LE, Schleiffer A, Mechtler K, Pauli A. Zebrafish Ski7 tunes RNA levels during the oocyte-to-embryo transition. bioRxiv 2020:2020.03.19.998716.

[73]. Xie T, Spradling AC. A Niche Maintaining Germ Line Stem Cells in the Drosophila Ovary. Science Reports 2000;290:328–30.

[74]. McCarthy A, Sarkar K, Martin ET, Upadhyay M, James JR, Lin JM, et al. MSL3 coordinates a transcriptional and translational meiotic program in female Drosophila. bioRxiv 2019:2019.12.18.879874.

[75]. Wineland DM, Kelpsch DJ, Tootle TL. Multiple Pools of Nuclear Actin. Anat Rec 2018;301:2014–36. doi:10.1002/ar.23964.

[76]. Gerbasi VR, Preall JB, Golden DE, Powell DW, Cummins TD, Sontheimer EJ. Blanks, a nuclear siRNA/dsRNA-binding complex component, is required for Drosophila spermiogenesis. Proceedings of the National Academy of Sciences 2011;108:3204–9. doi:10.1073/pnas.1009781108.

[77]. Upadhyay M, Martino Cortez Y, Wong-Deyrup SW, Tavares L, Schowalter S, Flora P, et al. Transposon Dysregulation Modulates dWnt4 Signaling to Control Germline Stem Cell Differentiation in Drosophila. PLoS Genet 2016;12. doi:10.1371/journal.pgen.1005918.

[78]. McCarthy A, Deiulio A, Martin ET, Upadhyay M, Rangan P. Tip60 complex promotes expression of a differentiation factor to regulate germline differentiation in female Drosophila. Molecular Biology of the Cell 2018;29:2933–45. doi:10.1091/mbc.E18-06-0385. [PubMed: 30230973]

[79]. Flora P, Schowalter S, Wong-Deyrup S, DeGennaro M, Nasrallah MA, Rangan P. Transient transcriptional silencing alters the cell cycle to promote germline stem cell differentiation in Drosophila. Developmental Biology 2018;434:84–95. doi:10.1016/j.ydbio.2017.11.014. [PubMed: 29198563]

[80]. Wang X, Page-McCaw A. Wnt6 maintains anterior escort cells as an integral component of the germline stem cell niche. Development (Cambridge, England) 2018;145. doi:10.1242/dev.158527.

[81]. Fuchs G, Diges C, Kohlstaedt LA, Wehner KA, Sarnow P. Proteomic analysis of ribosomes: translational control of mRNA populations by glycogen synthase GYS1. Journal of Molecular Biology 2011;410:118–30. doi:10.1016/j.jmb.2011.04.064. [PubMed: 21570405]

[82]. Bailey TL, Elkan C. Fitting a mixture model by expectation maximization to discover motifs in biopolymers. Proceedings of the Second International Conference on Intelligent Systems for Molecular Biology 1994;2:28–36.

[83]. Grant CE, Bailey TL, Noble WS. FIMO: scanning for occurrences of a given motif. Bioinformatics 2011;27:1017–8. [PubMed: 21330290]

[84]. Kim D, Langmead B, Salzberg SL. HISAT: a fast spliced aligner with low memory requirements. Nat Meth 2015;12:357–60.

[85]. Liao Y, Smyth GK, Shi W. featureCounts: an efficient general purpose program for assigning sequence reads to genomic features. Bioinformatics 2014;30:923–30. doi:10.1093/bioinformatics/btt656. [PubMed: 24227677]

[86]. Love MI, Huber W, Anders S. Moderated estimation of fold change and dispersion for RNA-seq data with DESeq2. Genome Biol 2014;15:550. [PubMed: 25516281]

[87]. Trcek T, Lionnet T, Shroff H, Lehmann R. mRNA quantification using single-molecule FISH in Drosophila embryos. Nat Protoc 2017;12:1326–48. [PubMed: 28594816]

[88]. Kim D, Langmead B, Salzberg SL. HISAT: a fast spliced aligner with low memory requirements. Nat Meth 2015;12:357–60.

[89]. Bailey TL, Williams N, Misleh C, Li WW. MEME: discovering and analyzing DNA and protein sequence motifs. Nucleic Acids Research 2006;34:W369–73. [PubMed: 16845028]

Highlights:

- Ski complex mediated RNA degradation is required in the germline for fertility.
- A subset of early oogenic RNAs are degraded concurrent with oocyte specification.
- Early oogenic RNAs are degraded utilizing components of the No Go Decay pathway.
- Degradation of early oogenic RNAs is required for maintenance of oocyte fate.

Inclusion and diversity

One or more of the authors of this paper self-identifies as an underrepresented ethnic minority in science. One or more of the authors of this paper self-identifies as a member of the LGBTQ+ community. One or more of the authors of this paper received support from a program designed to increase minority representation in science.

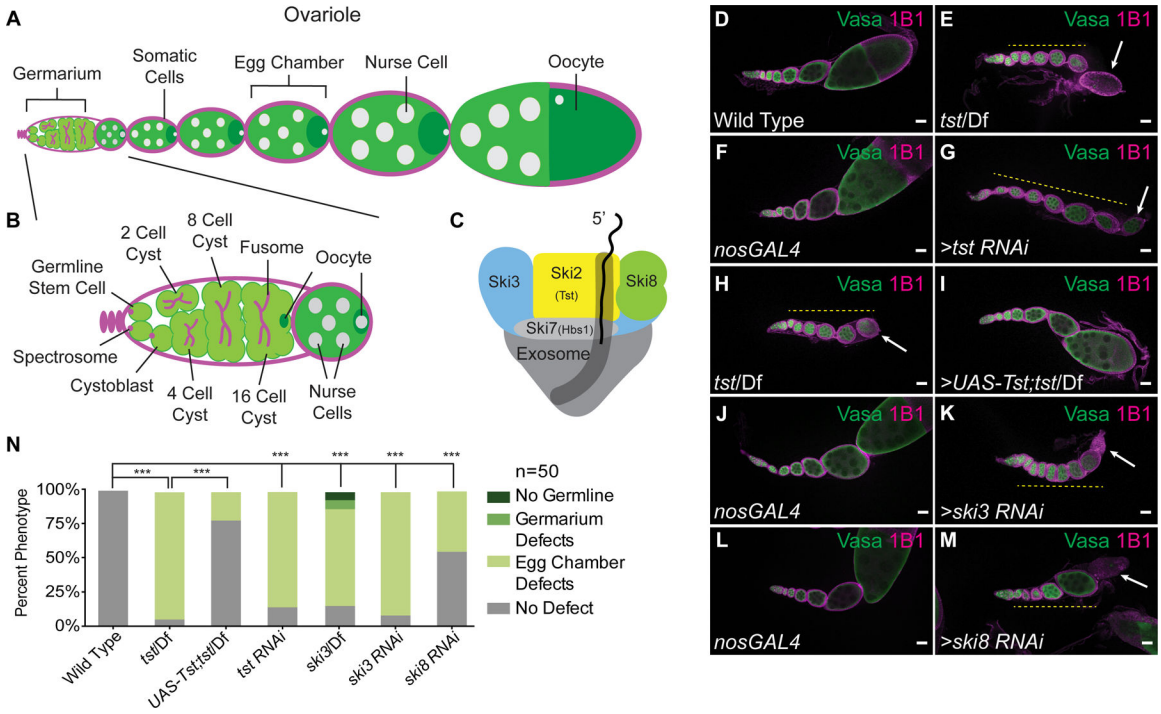

Figure 1. Components of the Ski Complex are required in the germ line for oogenesis.

(**A**) Schematic of a *Drosophila* ovariole and (**B**) germarium. (**C**) The Ski complex is composed of Ski2 (Tst, yellow), Ski3 (blue), Ski8 (green), and Ski7 (Hbs1, light gray) threading mRNA into the exosome (dark gray). (**D–M**) Confocal images of ovarioles stained with Vasa (green) and 1B1 (magenta). (**D**) Adult WT ovarioles show normal egg chamber development. (**E**) Hypomorphic *tst* genomic mutant ovariole displaying egg chambers that do not grow in size (yellow dashed line) and a dying egg chamber (arrow). (**F**) *nosGAL4* driver control ovariole shows WT morphology. (**G**) *tst* germline RNAi knockdown ovariole displaying egg chambers that do not grow in size (yellow dashed line) and a dying egg chamber (arrow). (**H**) *tst* genomic mutant ovariole (control for I) showing egg chamber defects (yellow dashed line) and dying egg chamber (white arrow) (**I**) *tst* genomic mutant ovariole expressing recombinant Tst protein in the germline rescues the egg chamber defects. (**J–M**) Germline RNAi knockdown for *ski3* (**K**) and *ski8* (**M**) also display egg chambers that do not grow in size (yellow dashed line) and dying egg chambers (arrow), whereas *nosGAL4* driver controls (**J, L**) have WT egg chambers. (**N**) Quantification of oogenesis defect phenotypes (n=50 ovarioles per genotype, *** = $p < 0.001$, Chi-squared tests with Bonferroni correction, df=3). *tst*/Df and *tst RNAi* are not significantly different. Scale bars = 10μm. See also Figure S1.

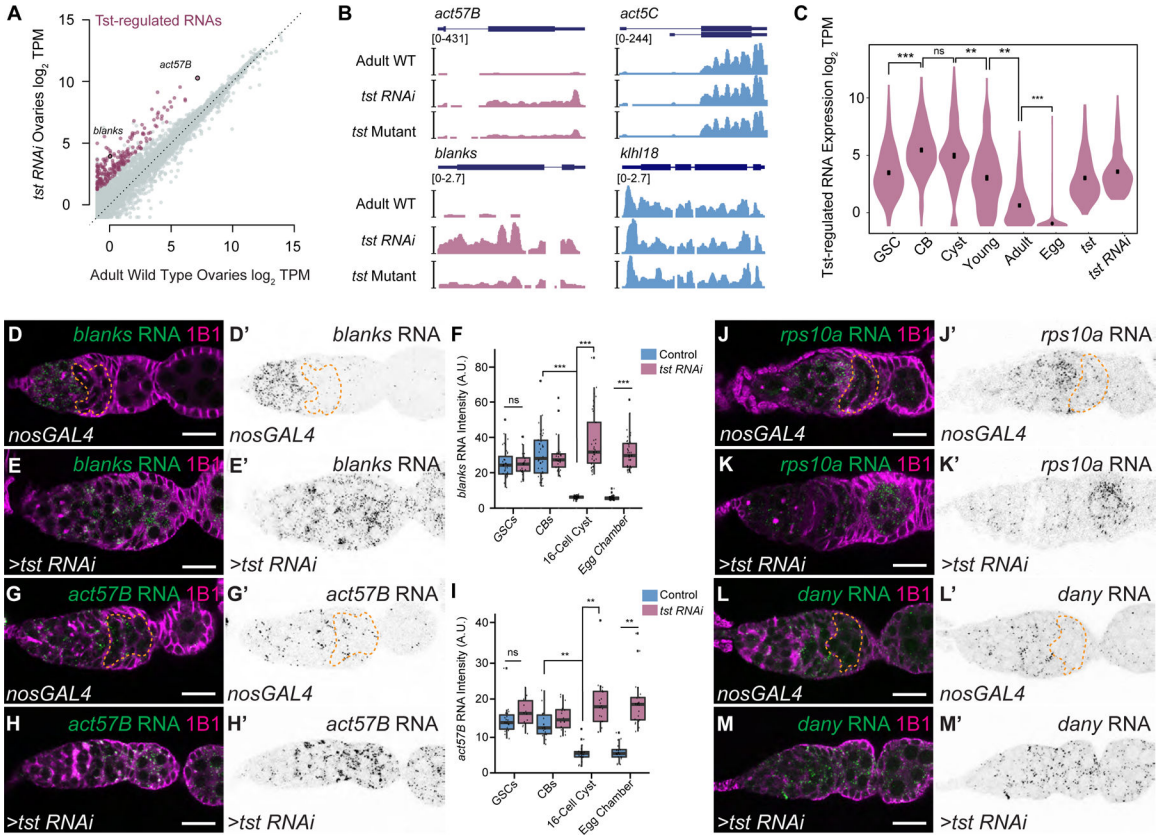

Figure 2. Twister promotes degradation of a subset of transcripts concurrent with oocyte specification.

(**A**) RNA-seq biplot comparing adult WT and *tst* germline RNAi knockdown ovaries showing upregulated Tst-regulated RNAs (magenta). *act57b* and *blanks* are highlighted. TPM = transcripts per million. (**B**) RNA-seq coverage tracks of Tst-regulated genes *act57B* and *blanks* (magenta) and non-targets *act5C* and *klhl18* (blue). (**C**) Violin plot of Tst-regulated RNAs (n=207) showing decrease in expression after differentiation and cyst stages. *** = p < 1e-25, Wilcoxon signed rank test with Bonferroni correction. GSC = germline stem cells, CB = cystoblasts. (**D–H**) Confocal images of *in situ* hybridizations probing for Tst-regulated RNAs *blanks* and *act57B* (green) and staining for 1B1 (magenta). (**D'-H'**) Corresponding *in situ* signals in grayscale. *blanks* RNA expression is restricted to undifferentiated cells and early cyst in a *nosGAL4* driver control (dotted orange line) (**D, D'**) but is expanded to egg chambers in *tst RNAi* ovarioles (**E, E'**). (**F**) Quantification of *blanks in situ* signal in different cell types in the ovariole. *** = p < 0.001, Tukey's post-hoc test (n=24–42 per cell type). Compared to *nosGAL4* control (**G, G'**), *act57B* RNA expression is also expanded in *tst RNAi* (**H, H'**). (**I**) Quantification of *act57B in situ* signal in different cell types in the ovariole. ** = p < 0.01, Tukey's post-hoc test (n=14–23 per cell type). Scale bars = 10μm. See Supplement for quantification for J–M'. A.U. = arbitrary units. See also Figure S2 and Data S1.

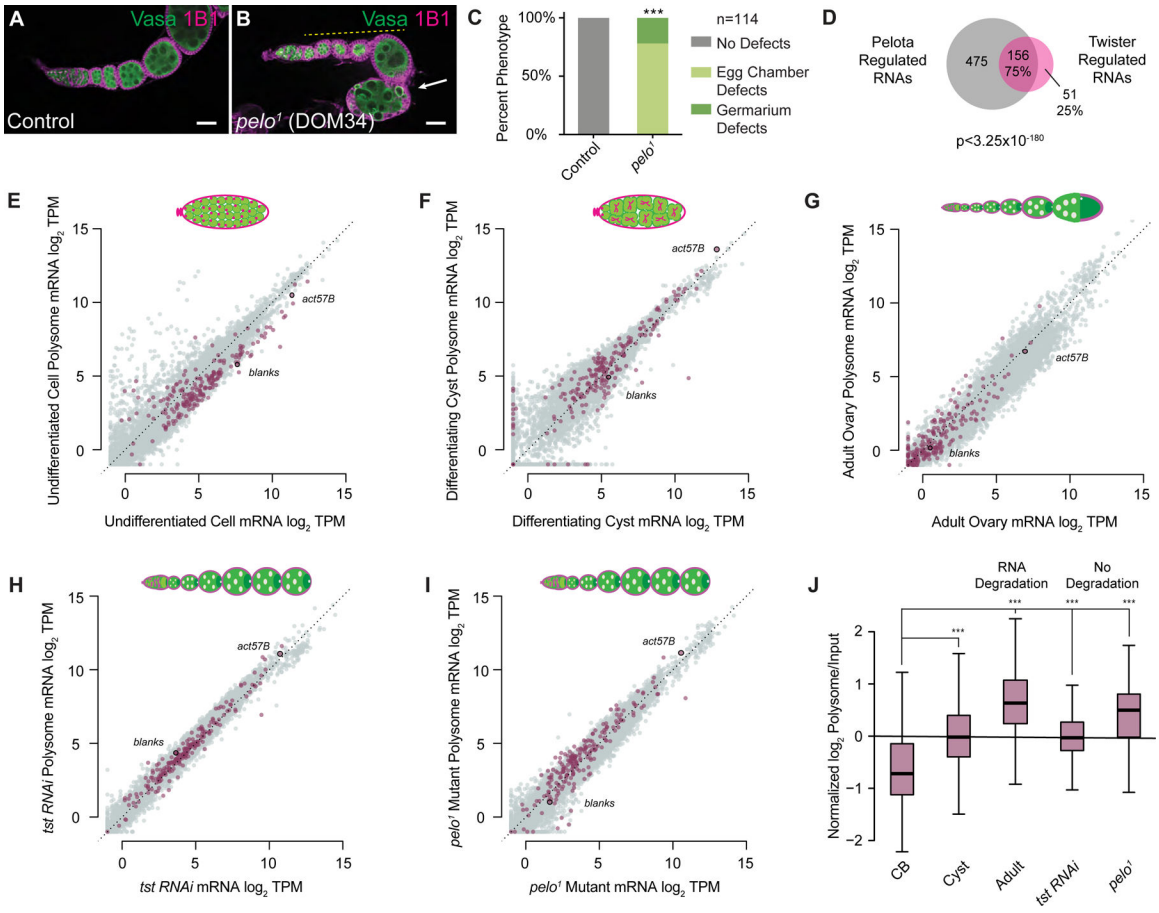

Figure 3. Twister-regulated RNAs are co-regulated by Pelota and exhibit an increased ribosome association concurrent with a decrease in RNA abundance.

(**A**) Confocal image of a WT control and (**B**) *pelo*^{1} mutant ovariole stained with 1B1 (magenta) and Vasa (green) and indicating egg chambers that fail to grow (yellow dashed line) and subsequently die (arrow). Scale bars = 10μm. (**C**) Quantification of oogenesis phenotypes observed in *pelo*^{1} mutants (n=114 ovarioles, $p < 0.001$, Chi-squared tests, df=2). (**D**) Venn diagram illustrating overlap of Tst-regulated RNAs that are >2 fold upregulated upon loss of *pelo* ($p < 3.25\times10^{-180}$, Hypergeometric Test). (**E–I**) Biplots of poly(A)+ mRNA Input versus polysome associated mRNA showing Tst-regulated RNAs (magenta) and highlighting Tst-regulated *blanks* and *act57B*. In undifferentiated germ cells (**E**) and differentiating cysts (**F**), Tst-regulated RNAs show high abundance and ribosome association compared to adult WT (**G**). Tst-regulated RNAs also have high abundance and ribosome association in germline *tst* RNAi (**H**) and *pelo*^{1} (**I**) ovaries. (**J**) Box plots of normalized $\log_2$ polysome/input mRNA of Tst-regulated RNAs across the samples. Overall ribosome association increases during the transition from CB to cyst to adult. Ribosome association in *tst RNAi* and *pelo*^{1} ovaries, where Tst-regulated RNA degradation is not occurring, is elevated compared to CB, but comparable to cyst. *** = $p < 0.001$, Estimated marginal means post-hoc tests on repeated-measures ANOVA. See also Figure S3 and Data S1.

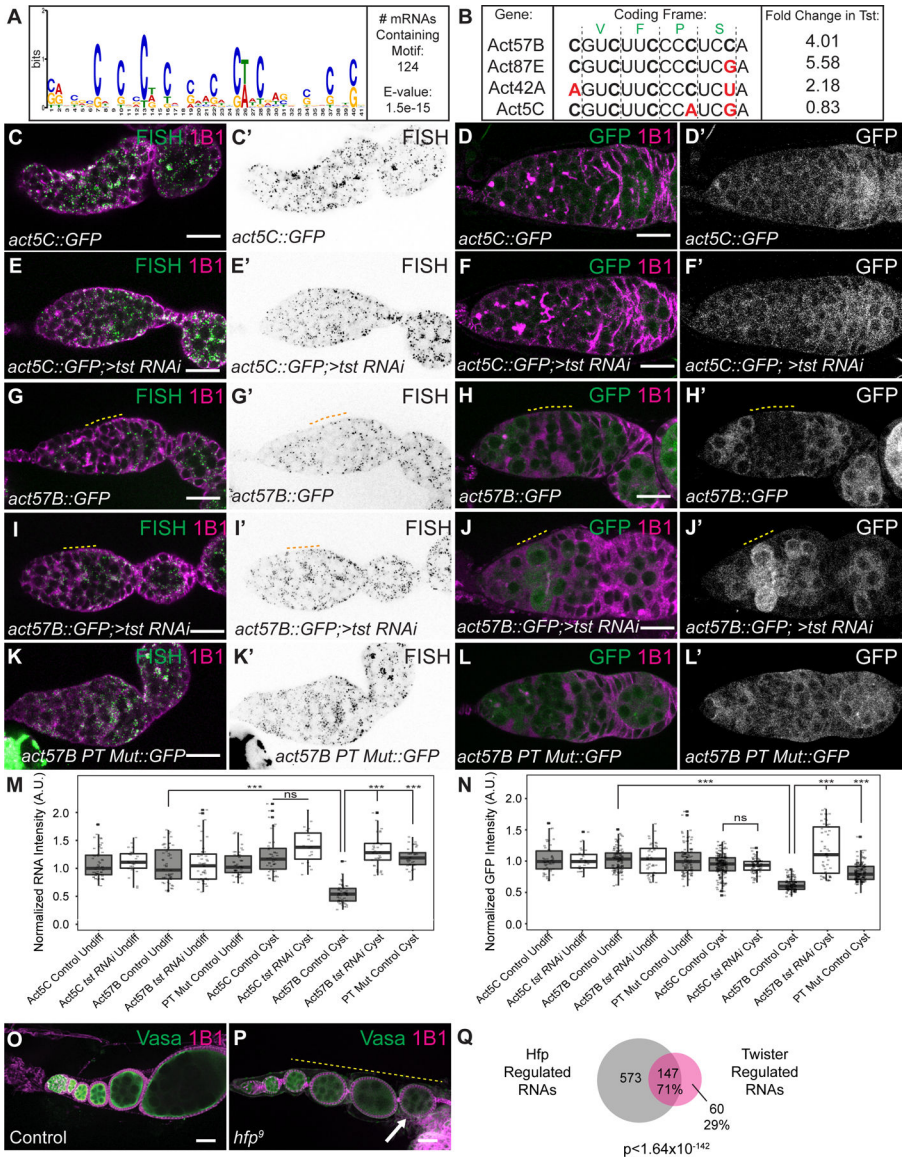

Figure 4. Twister-regulated RNAs are regulated by polypyrimidine rich sequence in their CDS and are regulated by Half Pint.

(**A**) Sequence logo of the polypyrimidine-rich motif identified by MEME to be enriched in the CDS of 124 Tst-regulated RNAs. (**B**) CDS alignment of Tst-regulated RNAs *act57B* and *act87E*, as well as *act42A* that is sensitive to *tst*, and non-target paralog *act5C*, showing divergent polypyrimidine-rich tracts (PTs). Black vertical lines indicate coding frame with amino acid symbols above. Fold-change increase in *tst* RNAi ovaries over WT is shown to the right. (**C–L'**) *in situ* hybridization and GFP fluorescence of reporters (green, grayscale) and 1B1 staining (magenta) in germaria. *act5C::GFP in situ* (**C–C'**) and GFP protein (**D–D'**) show uniform expression and do not change upon loss of *tst* (**E–F'**). *act57B::GFP in situ* (**G–G'**) and GFP protein (**H–H'**) expression are decreased in WT cyst stages (yellow dashed line) but expression is expanded into the cyst upon loss of *tst* (**I–J'**). *act57B::GFP* fusion with mutated PT shows ubiquitous expression in WT (**K–L'**). (**M**) Quantification of reporter RNA *in situ* intensity in undifferentiated cells and cyst stages (n=19–54 per cell type). *** =

$p < 0.001$, Tukey's post-hoc test. (**N**) Quantification of GFP intensity in undifferentiated cells and cyst stages (n=28–207 per cell type). *** = $p < 0.001$, Tukey's post-hoc test. A.U. = arbitrary units. (**O**) Confocal image of control and (**P**) *hfp*^{9} mutant ovariole stained with 1B1 (magenta) and Vasa (green) showing egg chambers that do not grow in size (yellow dashed line) and dying egg chamber (arrow). (**Q**) Venn diagram of Tst-regulated RNAs and Hfp regulated RNAs indicating that Tst and Hfp share 71% (147/208) of their target RNAs ($p < 1.64\times10^{-142}$, Hypergeometric Test). Scale bars = 10μm. See also Figure S4, Data S1 and S2.

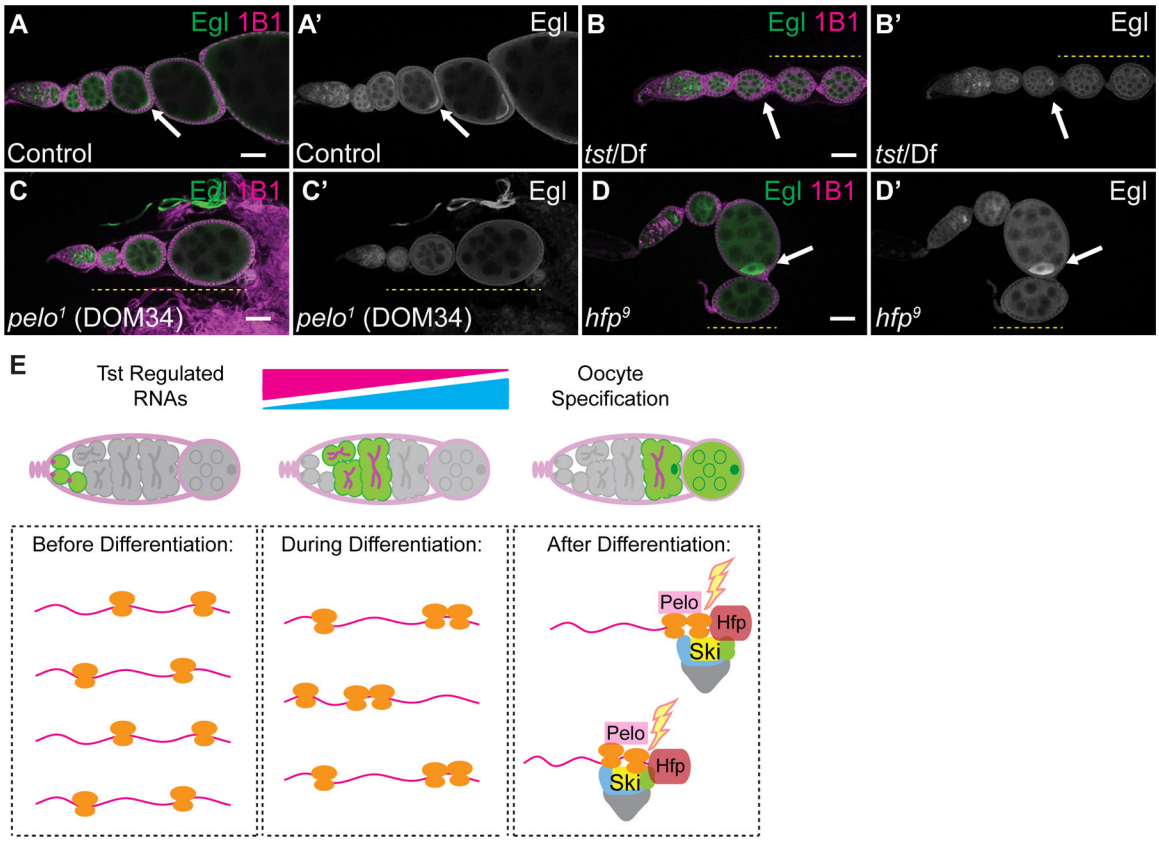

Figure 5. Twister is required for maintaining oocyte fate.

(**A–A'**) WT control, (**B–B'**) *tst*/Df, (**C–C'**) *pelo*^{1} and (**D–D'**) *hfp*^{9} mutant ovarioles stained with 1B1 (magenta) and Egl (green and grayscale) showing initial localization of Egl (arrow) and subsequent loss of Egl accumulation (yellow dashed line). Scale bars = 10μm. (**E**) In undifferentiated cells (left), Tst-regulated RNAs are highly expressed, yet lowly associated with ribosomes, and required for early oogenesis. During differentiation (center), ribosome association of Tst-regulated RNAs increases. After differentiation (right), during oocyte specification, Hfp protein binds in the CDS of Tst-regulated RNAs leading to targeting by Pelo, and the Ski complex. See also Figure S5 and Table S1.

KEY RESOURCES TABLE

REAGENT or RESOURCE	SOURCE	IDENTIFIER
Antibodies		
Rabbit polyclonal anti-GFP	abCam	ab6556
Mouse anti-1B1	Developmental Studies Hybridoma Bank	Antibody Registry ID: 528070
Rat monoclonal anti-HA high affinity	Roche Diagnostics	REF: 11867423001
Rabbit polyclonal anti-Vasa	Rangan Lab	N/A
Chicken polyclonal anti-Vasa	Rangan Lab	N/A
Rabbit polyclonal anti-Blanks	Gift from Sontheimer Lab	N/A
Mouse polyclonal anti-Actin C4	Sigma	MAB1501
Rabbit polyclonal anti-Cleaved Caspase 3	Cell Signalling	#96615
Rabbit polyclonal anti-Egalitarian	Gift from Lehmann Lab	N/A
Mouse polyclonal anti-Half pint	Gift from Schüpbach Lab	N/A
Anti-rabbit Alexa 488	Jackson ImmunoResearch Labs	Code:711–546-152
Anti-mouse Cy3	Jackson ImmunoResearch Labs	Code:715–546-150
Anti-chicken Alexa 647	Jackson ImmunoResearch Labs	Code:703–606-155
Anti-rabbit HRP	Jackson ImmunoResearch Labs	Code:111–035-144
Anti-mouse HRP	Jackson ImmunoResearch Labs	Code:115–035-003
Rabbit Anti-Orb	Gift from Lehmann Lab	N/A
Rabbit Anti-Fibrillarin	abCam	ab166630
Bacterial and Virus Strains		
DH5α competent *E. coli*	New England Biolabs Inc.	#C25271
XL-10 Gold Ultracompetent cells	Integrated Sciences	#200315
Chemicals, Peptides, and Recombinant Proteins		
Formaldehyde (Methanol Free), 10% Ultrapure	Polysciences Inc.	#04018–1
Donkey Serum	Sigma-Aldrich	SKU: D9663
Vectashield Antifade Mounting Medium with DAPI	Vector Laboratories	#H-1200
Triton X-100 detergent	VWR	#97062–208
Nonidet P-40 (NP-40) substitute	IBI Scientific	#9016–45-9
Tween-20 detergent	VWR	#97062–332
TRIzol	Invitrogen	#15596026
Complete, EDTA-free Protease Inhibitor Cocktail Pill	Sigma-Aldrich	SKU: 11873580001
Gibson Assembly Master Mix	New England Biolabs Inc.	E2611L
Restriction Endonuclease SpeI	New England Biolabs Inc.	R0133S
Gateway Clonase II	Invitrogen	#12535–029
Schneider's *Drosophila* Medium	Gibco	#21720024
Dynabeads Protein A	Invitrogen	#10002D
Bradford reagent	Bio-Rad	#500–0205
4X Laemmli Sample Buffer	Bio-Rad	#161–0747

REAGENT or RESOURCE	SOURCE	IDENTIFIER
SuperScript II	Invitrogen	18064022
Critical Commercial Assays		
TURBO DNA-free Kit	Life Technologies	AM1907
SYBR Green Master Mix	Applied Biosystems	#4367659
NEXTflex Rapid Illumina DNA-Seq Library Prep Kit	BioO Scientific	NOVA-5138–11
Click-iT EdU Cell Proliferation Kit	Invitrogen	C10337
RNAScope Kit	Advanced Cell Diagnostics	#310091
Mini-PROTEAN TGX 4–20% gradient SDS-PAGE gels	Bio-Rad	#456–1094
Western ECL Substrate	Bio-Rad	#1705060
Deposited Data		
RNA-Seq Data	This paper	GEO: GSE166275
RNA-Seq Data	[74]	GEO: GSE77294
RNA-Seq Data	[34]	GEO: GSE119458
RNA-Seq Data	[36]	GEO: GSE143728
Experimental Models: Organisms/Strains		
D. melanogaster: RNAi for *tst*: y^1 sc* v^1 sev^{21}; P{TRiP.HMC03796}attP40	Bloomington Drosophila Stock Center	BDSC: 55647
D. melanogaster: RNAi for *CG8777* (Ski3): P{KK106325}VIE-260B	Vienna Drosophila Resource Center	VDRC: v100948
D. melanogaster: *bam* Mutant: ry^{506} e^1 $bam^{\Delta 86}$/TM3, ry^{RK} Sb^1 Ser^1	Bloomington Drosophila Stock Center	BDSC: 5427
D. melanogaster: UAS-tkv: w*; P{UAS-tkv.Q253D.Nb}3/ TM3, Sb^1 Ser^1	Bloomington Drosophila Stock Center	BDSC: 36536
D. melanogaster: RNAi for *CG3909* (Ski8): y^1 sc* v^1 sev^{21}; P{TRiP.HMC04664}attP40	Bloomington Drosophila Stock Center	BDSC: 57377
D. melanogaster: RNAi for *bam*: y^1 v^1; P{TRiP.HMJ22155}attP40	Bloomington Drosophila Stock Center	BDSC: 58178
D. melanogaster: Heat shock *bam*: w^{1118}; P{hs-bam.O}11d/ TM3, Sb^1	Bloomington Drosophila Stock Center	BDSC: 24637
D. melanogaster: *nosGAL4* Driver: P{UAS-Dcr-2.D}1, w^{1118}; P{GAL4-nos.NGT}40	Bloomington Drosophila Stock Center	BDSC: 25751
D. melanogaster: *nosGAL4* Driver: UAS-Dcr2;nosGAL4;bamGFP	Lehmann Lab	N/A
D. melanogaster: *nosGAL4* Driver: If/CyO;nosGAL4	Lehmann Lab	N/A
D. melanogaster: *nosGAL4* Driver: y^1 w*; P{GAL4-nos.NGT}40	Bloomington Drosophila Stock Center	BDSC: 4442
D. melanogaster: tjGAL4 Driver: tjGAL4/CyO	Lehmann Lab	N/A
D. melanogaster: Wild type Control: y^1 w^{1118} P{70FLP}3F	Bloomington Drosophila Stock Center	BDSC: 6420
D. melanogaster: *tst* Mutant: w^{1118}; Mi{ET1}$tst^{MB10212}$/TM6C, Sb^1	Bloomington Drosophila Stock Center	BDSC: 29100
D. melanogaster: *hfp* Mutant: hfp^9,cu/TM2	Schüpbach Lab	N/A
D. melanogaster: Hfp-HA: *M{UAS-hfp.ORF.3xHA}ZH-86Fb*	FlyORF	F000989
D. melanogaster: Pelo-HA: *M{UAS-pelo.ORF.3xHA.GW}ZH-86Fb*	FlyORF	F003036

REAGENT or RESOURCE	SOURCE	IDENTIFIER
D. melanogaster: *CG8777* (Ski3) Mutant: y^1 w*; Mi{MIC}CG8777^{MI02824}	Bloomington Drosophila Stock Center	BDSC: 35904
D. melanogaster: *CG8777* (Ski3) Deficiency: *w[1118];Df(2R)ED1770,P{w[+mW.Scer\FRT.hs3]=3'.RS5+3.3'} ED1770/SM6a*	Bloomington Drosophila Stock Center	BDSC: 9157
D. melanogaster: *tst* Deficiency: *w[1118]; Df(3R)Exel9013/TM6B, Tb[1]*	Bloomington Drosophila Stock Center	BDSC: 7991
D. melanogaster: *pelo* Mutant: *$pelo^1$/CyO*	Bloomington Drosophila Stock Center	BDSC: 11757
Oligonucleotides		
Primers for qRT-PCR see Table S4	This paper	N/A
Primers for Gateway Cloning see Table S4	This paper	N/A
RNAScope Probe Against *blanks*	Advanced Cell Diagnostics	Base pairs 29–1250 NM_139709.2
RNAScope Probe Against *act57B*	Advanced Cell Diagnostics	Base pairs 1196–1693 NM_079076.4
RNAScope Probe Against *dany*	Advanced Cell Diagnostics	Base pairs 213–1141 NM_166493.2
RNAScope Probe Against *rps10a*	Advanced Cell Diagnostics	Base pairs 2–599 NM_143319.4
GFP RNA FISH probe labeled with CALFluor590	[87]	N/A
Recombinant DNA		
Plasmid: pCaSpeR2 P element transformation vector	Drosophila Genomics Resource Center	Stock Number: 1066
Gateway Destination Vector Plasmid: pPWG	Drosophila Genomics Resource Center	Gateway 1 Collection
Gateway Destination Vector Plasmid: pPGW	Drosophila Genomics Resource Center	Gateway 1 Collection
Act5C Coding Sequence gBlock	Integrated DNA Technologies	NM_001297986.1
Act57B Coding Sequence gBlock	Integrated DNA Technologies	NM_079076.4
Act57B Mutant Coding Sequence gBlock	Integrated DNA Technologies	N/A
Gateway pDONR Vector	Invitrogen	#12536–017
Software and Algorithms		
ImageJ	NIH	https://imagej.nih.gov/ij/
HISAT2	[88]	https://ccb.jhu.edu/software/hisat2/index.shtml
DESeq2	[86]	http://www.bioconductor.org/packages/release/bioc/html/DESeq2.html
featureCounts	[85]	http://bioinf.wehi.edu.au/featureCounts/
FIMO	[83]	https://meme-suite.org/meme/doc/fimo.html
MEME Suite	[89]	https://meme-suite.org/doc/overview.html.